

Don't Get Me Wrong: How to apply Deep Visual Interpretations to Time Series

Christoffer Löffler, Wei-Cheng Lai, Björn M. Eskofier & Dario Zanca

Machine Learning and Data Analytics Lab

Friedrich-Alexander University Erlangen-Nuremberg

Carl-Thiersch-Straße 2b, 91052, Erlangen, Germany

{CHRISTOFFER.LOEFFLER, WESLEY.LAI, BJOERN.ESKOFIER, DARIO.ZANCA}@FAU.DE

Lukas Schmidt & Christopher Mutschler

Fraunhofer IIS, Fraunhofer Institute for Integrated Circuits IIS

Positioning and Networks Division

Erlangen, Germany

{LUKAS.SCHMIDT, CHRISTOPHER.MUTSCHLER}@IIS.FRAUNHOFER.DE

Abstract

The correct interpretation and understanding of deep learning models is essential in many applications. Explanatory visual interpretation approaches for image and natural language processing allow domain experts to validate and understand almost any deep learning model. However, they fall short when generalizing to arbitrary time series data that is less intuitive and more diverse. Whether a visualization explains the true reasoning or captures the real features is difficult to judge. Hence, instead of blind trust we need an objective evaluation to obtain reliable quality metrics. We propose a framework of six orthogonal metrics for gradient- or perturbation-based post-hoc visual interpretation methods designed for time series classification and segmentation tasks. An experimental study includes popular neural network architectures for time series and nine visual interpretation methods. We evaluate the visual interpretation methods with diverse datasets from the UCR repository and a complex real-world dataset, and study the influence of common regularization techniques during training. We show that none of the methods consistently outperforms any of the others on all metrics while some are ahead at times. Our insights and recommendations allow experts to make informed choices of suitable visualization techniques for the model and task at hand.

Keywords: explainable AI, time series, deep learning, evaluation metrics, visual interpretation.

1. Introduction

Due to its high performance on complex multi-modal data, deep learning (DL) becomes increasingly popular in many real-world applications that process time series data (Fawaz et al., 2019b). While we fundamentally rely on the networks' correct operation in many applications that consider safety (Berkenkamp et al., 2017) they remain difficult to interpret. Typical applications are the monitoring of industrial processes (Löffler et al., 2021), the support of healthcare and sports (Dorschky et al., 2020), or safety in autonomous driving (Schmidt et al., 2021). The need for improved model understanding (Carvalho et al.,

2019), along with regulatory guidelines (Goodman and Flaxman, 2017), led to a myriad of new approaches to the visual interpretation problem (Zhang and Zhu, 2018).

Post-hoc visual interpretation allows a domain expert to validate and understand how (almost) arbitrary deep learning models operate. Their central idea is highlighting features on the input that are "relevant" for the prediction of a learned model (Adebayo et al., 2018). Many of these techniques do not require a modification of the original model (Simonyan et al., 2014; Ribeiro et al., 2016) which makes them compatible with different architectures. Thus, they are useful as a general-purpose validation tool for neural networks across different tasks (Arrieta et al., 2020).

However, while visual interpretation yields intuitive and correct explanations for images (Samek et al., 2021), the application of these methods on time series data is still an unsolved problem (Rojat et al., 2021). Time series are inherently more diverse (Rojat et al., 2021) because they may originate from a variety of different sensors and processes, and often do not allow an obvious patch- or texture-based localization of critical features for human observers. This makes the application and the evaluation of visual interpretability methods difficult. A domain expert can not easily judge if explanations are correct in (i) delivering the reasoning of the decision process in the DL model and in (ii) capturing the real features in the dataset that lead to a correct classification.

Hence, it is important not to blindly apply different visualization methods. This requires quality metrics that evaluate visual interpretations and that enable an expert to select a suitable visualization for a given model and task at hand. However, both state-of-the-art visualization techniques and metrics that evaluate visual interpretations, e.g., Pixel Flipping (Samek et al., 2017), Sanity Check (Adebayo et al., 2018), and sensitivity checks (Rebuffi et al., 2020), so far have been examined on images (Rojat et al., 2021) or on NLP tasks (Arras et al., 2017), but only rarely on more diverse time series (Schlegel et al., 2019). This lack of objective and subjective evaluation seriously limits their application and utility for time series.

This paper provides a study of six orthogonal metrics that characterize the quality of visual interpretations for time series data. We investigate "sanity" (Adebayo et al., 2018), "faithfulness" (Alvarez Melis and Jaakkola, 2018; Schlegel et al., 2019), "sensitivity" (Rebuffi et al., 2020), "robustness" (Yeh et al., 2019), "stability" (Fel and Vigouroux, 2020; Li et al., 2021), and a novel metric based on annotations: "localization". These metrics rate and validate distinct qualities of saliency. We further investigate how training choices and conditions, like the dataset, model architecture, and regularization methods, modify the quality and characteristics of visual interpretations. Based on this investigation, we give clear recommendations that allow experts to choose and validate appropriate visualization methods for time series data.

In our extensive evaluation, we train four different architectures on two different types of tasks: U-Time (Perslev et al., 2019) and bidirectional Long Short-Term Memory (bi-LSTM) (Schuster and Paliwal, 1997) on segmentation tasks, and Fully Convolutional Network (FCN) (Long et al., 2015) and Temporal Convolutional Network (TCN) (Bai et al., 2018) on classification tasks. We use diverse datasets from the UCR repository (Dau et al., 2018) (GunPointAgeSpan, FordA, FordB, ElectricDevices, MelbournePedestrian, NATOPS) for classification and the more complex real-world tool tracking dataset (Löffler et al., 2021) for segmentation. Additionally, we evaluate the effects of dropout, ℓ_1 , and ℓ_2

regularization. The experiments show the necessity of all categories to create an objective rating for methods, models and tasks, and highlight the importance of the regularization technique during model training. Our recommendations help domain experts to understand, rate, and validate saliency for time series in safety-critical applications.

The remainder of this article is structured as follows. Section 2 discusses background and related work. Section 3 introduces extended and novel metrics for both the classification and segmentation task. Section 4 discusses our experimental results. Based on these findings, Section 5 proposes recommendations. Section 6 concludes.

2. Background and Related Work

Interpretation methods for DL models can be divided into ante-hoc methods, that are inherently part of the model, and post-hoc methods, that provide the interpretation after training (Rojat et al., 2021). We focus on post-hoc methods and divide them into gradient-based and perturbation-based methods (Li et al., 2021; Warnecke et al., 2020; Ismail et al., 2020).

Gradient-based methods compute the relevance for all input features by passing gradients backwards through the neural network (Ancona et al., 2018). *Gradient* (Simonyan et al., 2014) computes the saliency map M^c of a class c using the derivative of the class score P^c of the model with respect to the input sample x , as $M^c(x) = \frac{\partial P^c}{\partial x}$. The gradient indicates the importance of points in the input sequence for predictions. The advantage of gradient-based methods lies in their computational efficiency, as they use only a small number of backward passes to compute $M^c(x)$.

Perturbation-based methods perturb known input samples and measure the effects of specific perturbations on the predicted class via a forward pass through the network. For instance, Local Interpretable Model-Agnostic Explanations (LIME) (Ribeiro et al., 2016) fits a local surrogate model (e.g., a linear regression) as an explanation, and calculates relevance based on this surrogate. Perturbation-based methods are computationally expensive as they require multiple forward passes per sample. However, they do not need gradient information and hence also work with black-box models.

2.1 Metrics for Saliency on Time Series

Most interpretation methods were originally designed for image or text data. Understanding and comparing visual interpretation is intuitive on image data, compared to more abstract time series. Furthermore, the diversity of interpretation methods complicates an objective choice for the model and task (Rojat et al., 2021). For example, when Wang et al. (2017) and Fawaz et al. (2019b) apply Class Activation Maps (CAM) (Zhou et al., 2016) on well-known UCR datasets (Dau et al., 2018), they notice a qualitative difference of CAM interpretations between network architectures. This suggests that the difference in quality should be quantified. Similarly, other work relies on domain experts that perform a (costly) qualitative evaluation that is costly compared to an algorithmic one (Strodthoff and Strodthoff, 2019; Fawaz et al., 2019a; Oviedo et al., 2019). Hence, there is an increasing need for objective evaluation metrics to make the interpretations’ quality measurable and comparable.

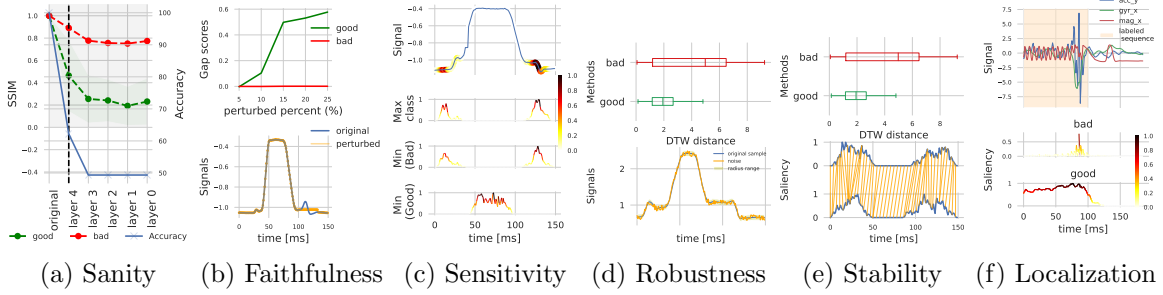


Figure 1: We show examples for a good (green) and a bad (red) score for each metric: (a) sane saliency depends on network parameters, tested by randomizing weights and biases; (b) faithful saliency correlates with predictive accuracy, tested by perturbing the input sequence; (c) sensitive saliency of the predicted class in one sample is different from others; (d) for robust saliency small changes to input data cause only small effects; (e) stable saliency assigns relevance to similar features for the same class; (f) saliency should be localized on the predicted segment.

2.2 Categories of Metrics

Metrics can be divided into different categories, depending on the question they answer. Doshi-Velez and Kim (2017) propose a distinction between *human-grounded* and *functional* metrics. The former involve human perception and intuition with the goal of generating qualitative, intuitive visualizations, e.g., bounding boxes for image object detection for testing the localization of saliency maps (Jianming et al., 2016), or questionnaires to indicate participants’ opinions on the quality of explanations (Li et al., 2021). Functional metrics provide statistical measures that aim to capture true model behavior instead, e.g., to aggregate performance metrics automatically (Rojat et al., 2021), and make use of proxy tasks to generate a quantitative evaluation. Another categorization (Li et al., 2021) identifies multiple broad categories for image data, that we may transfer to time series, i.e., the faithfulness of salient features, the class sensitivity of an explanation, and the stability of explanations given noisy inputs.

This article proposes a framework of metrics with orthogonal categories, specifically to time series. We adapt and extend metrics to (multivariate) time series and propose an intra-class stability metric and a concept of relevance localization: we build on the pointing game (Jianming et al., 2016) and combine it with the precision and recall for time series framework (Tatbul et al., 2018). Furthermore, we provide an in-depth evaluation and discussion of saliency methods and the influence of regularization on time series classification.

3. Scoring Categories

We propose a set of six distinct categories (sanity, faithfulness, sensitivity, robustness, stability, and localization) to assess visual interpretation methods and to determine their performance and trustworthiness in classification or segmentation tasks on time series. For each of them we propose a metric that enables a comparative evaluation of diverse types of visual interpretation methods.

Why do we need six scoring categories?

It seems tempting to rely on a single metric or on a single aggregated score across multiple metrics to assess the quality of a visual interpretation. However, we show that the six presented categories are orthogonal (see Fig. 2) and capture distinct qualities. Interpretations depend on model parameters (sanity check (Adebayo et al., 2018)), predictive features (faithfulness (Alvarez Melis and Jaakkola, 2018)), coherence of class predictions (intra-class stability (Fel and Vigouroux, 2020)), robustness against noise (max sensitivity with adversarial noise (Yeh et al., 2019)), specific sequences (or even points) in a time series like by Tatbul et al. (2018) (novel localization metric), and the relevance map’s specificity (inter-class sensitivity (Rebuffi et al., 2020)). It is important to assess if a given interpretation accurately captures these dependencies.

We give a brief overview of our framework’s metrics in Fig. 1:

- (a) *sane saliency* depends on network parameters and is structurally different after randomizing the network’s weights ρ_i for layers $[1, 2, 3]$ (Adebayo et al., 2018).
- (b) *faithful saliency* correlates with predictive accuracy. Perturbing a percentage of the input sequence with high saliency decreases accuracy (Alvarez Melis and Jaakkola, 2018).
- (c) saliency is *sensitive* if the predicted (max) class in one sample is sufficiently different from any other (min) class (Rebuffi et al., 2020).
- (d) saliency is *robust*, if small changes to the input cause only small changes to the saliency (Yeh et al., 2019).
- (e) saliency is *stable* if it assigns relevance to similar features for all samples of a class, with respect to a suitable distance metric (Fel and Vigouroux, 2020).
- (f) saliency should be *localized* on the segments of the predicted classes (t_0 to t_1).

Notation. We first introduce a unified notation that we adapt from Fawaz et al. (2019b): A multivariate time series is defined by $X = [X^1, \dots, X^H]$, where H is the number of input channels, $X^i = (x_1^i, \dots, x_T^i) \in \mathbb{R}^T$ is an ordered set of real values, and T denotes the number of time steps. For $H = 1$, we consider a *univariate* time series, otherwise we consider a *multivariate* time series. Time series often include complex temporal dependencies, i.e., distinct points are not independent. Time series classification defines a mapping $X \rightarrow y$ that minimizes the error on a dataset $D = \{(X_1, y_1), \dots, (X_N, y_N)\}$, where N is the number of data samples, $X \in D$ is a time series, $y_i \in \mathbb{R}^C$ denotes the one-hot vector of a class label the input belongs to, and C is the number of classes. In time series segmentation, we search $X \rightarrow Y$ that maps an input sample to a dense classification $Y = [y_1, \dots, y_T] \in \mathbb{R}^{C \times T}$ (Perslev et al., 2019), i.e., a class label is predicted for each time step. Post-hoc visual interpretation methods compute a relevance map $M_m^c \in \mathbb{R}^{H \times T}$, $M_m^c(X) = [R^1, \dots, R^H]$, where $R^i = (r_1^i, \dots, r_T^i)$, representing the importance of each input feature with respect to the class c and a model m , for each time step. We use M as a function to produce the

Faithfulness TI	1	0.1	0.1	-0.16	0.35
IC. Stability	0.1	1	0.25	-0.24	-0.13
Robustness	0.1	0.25	1	-0.2	0.11
Sanity	-0.16	-0.24	-0.2	1	0.028
Sensitivity	0.35	-0.13	0.11	0.028	1
	Faithfulness TI	IC. Stability	Robustness	Sanity	Sensitivity

Figure 2: Pairwise Pearson correlations of scores. Every metric is independent of all others.

saliency map. For clarity, we will omit the dependency on m , i.e., $M_m^c \equiv M^c$, if it is not explicitly required. An evaluation metric for visual interpretation methods defines a score $\mathcal{S}_{\text{metric}}(\cdot)$ that rates the quality of the relevance map M at a sample X given a model m and optional parameters. We provide a unified view, so that for all scores, a higher score corresponds to a better visualization according to the perspective.

3.1 Sanity

The sanity metric measures the idea that a visual interpretation depends on the model that is interpreted. Intuitively, if the weights and biases of a trained network model were re-initialized with random values, the network’s predictions and generated saliency maps should also be different from the original maps. However, this is not always the case. Despite a drop in model accuracy, saliency may remain stable. Hence, we test sanity using a variant of sanity check (Adebayo et al., 2018), that performs a *layer-wise cascading randomization* of the network’s weights and biases, starting from the output to the input. In contrast to independent randomization, the cascading approach results in a mostly continuous performance degradation of predictions, see Fig. 1a for an illustration. Network accuracy should increasingly resemble a random guessing. Following Adebayo et al. (2018), we compare saliency using the structural similarity index measure (SSIM) (Wang et al., 2004), that compares the distribution of sub-sequences of M^c . We define the sanity score as

$$S_{\text{Sanity}}(M, D, m) = -\frac{1}{N} \cdot \sum_{X \in D} \sum_{i=1}^L \frac{\text{SSIM}(M_m^c(X), M_{m_i}^c(X))}{L}, \quad (1)$$

where $|D| = N$, i enumerates the L layers of m , whose parameters are randomized and $M_{m_i}^c(x)$ is the saliency map after randomizing layer i of m . We average the SSIM over L layers and compute the average over all samples in D .

3.2 Faithfulness

A relevance measure is faithful, if input features with a high relevance (w.r.t. M^c) have a high influence on the model prediction, see Fig. 1b for an illustration. Alvarez Melis and Jaakkola (2018) propose a perturbation-based metric that evaluates the faithfulness of predictions. The metric measures the correlation between input (features) with high saliency on the one hand and predictive accuracy on the other hand. For time series data, there are two variants of faithfulness that are based on different assumptions of the data distribution. Both rank inputs of time step of $X_T \in \mathbb{R}^T$ according to the relevance of its saliency map. However, they differ in perturbations: Alvarez Melis and Jaakkola (2018) (further called Temporal Importance (TI)) strictly adhere to the ranked importance of saliency to choose what to perturb, while Schlegel et al. (2019) assume temporal correlation of inputs and perturb a connected sub-sequence instead (Temporal Sub-sequences (TS)). While the latter is a more intuitive model for perturbations on time series data, it may misrepresent importance of features, e.g., if they are not clustered or do not follow the assumption that they should be sequential. Furthermore, there may be several crucial sub-sequences in a single sample.

We use either variant of faithfulness on multivariate data X_T^H as follows. Based on the relevance r , we select time points $t \in \{1, \dots, T\}$ and features $i \in \{1, \dots, H\}$. For TI, we select and perturb the inputs of the sample X with highest relevance r_t^i and replace

their values with a mean value of the test dataset at time t . For TS, we select t according to the maximum relevance r_t^i and perturb a sub-sequence of the inputs of the sample X by replacing its values with a mean value of the test dataset of length L at time t , as $x_{\text{mean}} = (x_{t+\frac{L}{2}}^i, \dots, x_t^i, \dots, x_{t-\frac{L}{2}}^i)$, to break the temporal correlation.

The perturbed sample is denoted as X' . We compute the mean faithfulness scores over the whole dataset D for TI as

$$S_{\text{Faithfulness TI}}(M, D, m) = -\frac{1}{N \cdot L} \sum_{X \in D} \sum_{l=0}^L m^c(X'_l) \quad (2)$$

and for TS as

$$S_{\text{Faithfulness TS}}(M, D, m) = \frac{1}{N} \cdot \sum_{X \in D} m^c(X) - m^c(X'), \quad (3)$$

where $m^c : R^c \rightarrow R$ is the softmax prediction of the target class c . For TS the gap score between the softmax prediction of the original and the perturbed sample is $m^c(X) - m^c(X')$. For TI we use the Area Under Curve (AUC) instead, where L is the total perturbation length and X'_l is the perturbed sample at step l .

3.3 Inter-Class Sensitivity

In multi-class prediction tasks the classifier needs to identify relevant features for each of the classes to make a correct prediction. Hence, the relevance map M^c should identify different salient features for those different classes (Li et al., 2021), see Fig. 1c. If a method is not sensitive to the class, the score may indicate that the saliency is misleading, or that the classifier failed to learn correct features for these classes, and the sensitivity score should raise a red flag. Concretely, inter-class sensitivity (Rebuffi et al., 2020) measures class specific sensitivity of the generated relevance map with respect to the most likely (c_{\max}) and least likely (c_{\min}) class according to the model. We compute the mean inter-class sensitivity score as

$$S_{\text{Inter-Class Sensitivity}}(M, D) = -\frac{1}{N} \cdot \sum_{X \in D} \text{sim}(M^{c_{\max}}(X), M^{c_{\min}}(X)). \quad (4)$$

We compute similarity of two saliency maps as $\text{sim}(M^{c_{\max}}(x), M^{c_{\min}}(x))$ where $\text{sim}(\cdot, \cdot)$ is a similarity function (e.g., a cosine similarity) that is easy to interpret via its geometric interpretation. It is defined as the angle between two non-zero vectors that measures the similarity between their inner product space (Han et al., 2012). Similarity of M in binary classification would result in a negative cosine similarity, meaning nearly inverted saliency maps for max- and min-classes.

The sensitivity of the saliency map is not always strictly related to how well the saliency method captures model behavior. Saliency methods of low faithfulness could introduce their bias to the sensitivity score and hide true model behavior. However, inter-class sensitivity is still a useful indicator for the quality of a model and visualization, with the important caveat that a score is only meaningful if the visualization is both faithful and sane. See Section 5 for further details and recommendations on this.

3.4 Robustness

Recently, Dombrowski et al. (2019) showed the vulnerability of saliency methods to adversarial attacks. For reliable interpretations, saliency methods should be as robust to small

changes in the input as the model itself. We evaluate a method’s robustness with respect to adversarial noise (Yeh et al., 2019) via its sensitivity of the most likely class (c_{\max}), see Fig. 1d for an illustration. Intuitively, even with noisy inputs the saliency map of a model should not change significantly (Alvarez-Melis and Jaakkola, 2018) and saliency maps with high sensitivity are less reliable. Yeh et al. (2019) define the sensitivity of the saliency map derived from the gradient as

$$[\nabla_X M^c(X)]_j = \lim_{\epsilon \rightarrow 0} \frac{M^c(X + \epsilon e_j) - M^c(X)}{\epsilon} \quad (5)$$

for any $j \in \{1, \dots, |H \cdot T|\}$, where $e_j \in \mathbb{R}^{H \times T}$ is the j -th coordinate vector and the j -th entry is one while the others are zero. We use Monte Carlo sampling of ϵe_j , where $|\epsilon e_j| < a$ (a is a user-specified radius), to generate different $\hat{X} = X + \epsilon e_j$. We compare \hat{X} with the original X to compute

$$S_{\text{Max Sensitivity}}(M^c, D, a) = -\frac{1}{N} \cdot \sum_{X \in D} \max_{\|\hat{X} - X\| < a} \|M^c(\hat{X}) - M^c(X)\|. \quad (6)$$

In summary, evaluating the robustness of saliency methods should not hide the robustness, or lack thereof, of underlying models. Especially if these models are not robust themselves, saliency methods should accurately reflect their vulnerable behavior. Hence, robustness of saliency methods and models should be jointly evaluated.

3.5 Intra-Class Stability

Fel and Vigouroux (2020) propose algorithmic stability measures to test whether saliency methods produce similar interpretations for samples from the same class. Two explanations of the same feature should be similar, independent of their exact location within the input sample. This is helpful for generalization, as features may be translation-invariant.

To be able to compute this metric, we need to make several assumptions. First, we assume that the order of temporal features is correlated between different samples of the same class. Overall, this is a reasonable assumption, since time series data often contains distinct temporal features that follow a dataset-specific order. However, note that scores for intra-class stability are highly dataset-specific, and should not be compared across different datasets. See Fig. 4 for this evaluation. Second, we assume that the visualization method is faithful, and that both the visualization and the model are robust. This assumption has to be validated for every combination of model and visualization technique.

Based on these assumptions, we can test the intra-class stability of saliency maps M^c for a given dataset D using distance statistics, see Fig. 1e for an illustration. Specifically, we compute pairwise distances between saliency maps M^c for different samples $X_i, X_j \in D$ and aggregate these across classes:

$$S_{\text{Intra-Class Stability}}(M^c, D) = -\sum_{i \in [0, N]} \sum_{j \in [i+1, N]} \frac{d_{\text{dtw}}(M^c(D_i), M^c(D_j))}{N \cdot (N-1)}. \quad (7)$$

We use Dynamic Time Warping (DTW, Vintsyuk (1968)) as the distance function d_{DTW} . The score compares each classes’ sample’s M^c with all other samples’ saliency maps in the dataset, using d_{DTW} . DTW provides a crucial benefit by allowing us to compare time series that have similar features in the same order, but not on the exact-same point in time.

3.6 Localization

The temporal location of class-specific features with high relevance in a time series segmentation task should intuitively be situated within (or close-by) its labeled segment (temporal sub-sequence). This labelled sequence should also determine the location of saliency for models, see Fig. 1f for an illustration. Localization is a novel metric that measures this notion and allows experts to uncover potential problems in model-operation like shortcut learning.

Similar to intra-class stability, localization requires a faithful visualization. Additionally (but somewhat obviously), accurate labels are needed to compute a meaningful score. Given a faithful visualization, samples with lower scores (lower overlaps) warrant closer inspection. A low localization indicates spurious correlations due to unexpected features outside of the labeled sequence and can also help pinpoint faulty labels.

Our metric is an extension of the Pointing Game (Jianming et al., 2016) metric, that was previously used for object detection, to time series using range-based metrics (Tatbul et al., 2018). Localization systematically analyzes the saliency maps’ ranges in segmentation tasks. We argue that Pointing Game’s original hit-and-miss accuracy is inadequate for time series methods, as segmentation is point-wise exact. Thus, we replace it with range-based testing, yielding localization. This extension with front, middle and back biases can help uncover problematic issues such as temporal biases within the labeled sub-sequence or imprecise margins of the labels themselves. Furthermore, the metric may hint at learned shortcuts outside of the labeled sequence.

We compute localization as follows. First, we filter out non-relevant predictions (according to the relevance map). A prediction at time t , denoted with $\hat{Y}(t)$, is relevant if there exists an $i \in \{1, \dots, M\}$ such that $r_t^i > \max(|r|) \cdot \theta$ where θ is a value between $[0, 1]$. We select the model’s predicted class at time t if the prediction is relevant, otherwise we set the class to *none*. The resulting *relevancy-filtered* prediction is denoted as \hat{Y}' . Finally, we can compare \hat{Y}' with the ground truth Y and evaluate how well high saliency features lie within the annotated sub-sequences (Tatbul et al., 2018).

To compute the mean localization score for the whole dataset D , we compare any of the N_{sub} existing labeled sub-sequence $Y_{\text{sub}_i} \in R^T$ from D each with its temporally co-located prediction \hat{Y}'_i

$$S_{\text{localization}}(Y, \hat{Y}') = \sum_{i=0}^{N_{\text{sub}}} \frac{S_{\text{recall}}(Y_{\text{sub}_i}, \hat{Y}'_i)}{N_{\text{sub}}}. \quad (8)$$

For each pair $(Y_{\text{sub}_i}, \hat{Y}'_i)$ we calculate a range-based recall score based on the point-wise comparison proposed by Tatbul et al. (2018) as

$$S_{\text{recall}}(Y_{\text{sub}}, Y') = \alpha \cdot \text{existence}(Y_{\text{sub}}, Y') + (1 - \alpha) \cdot \text{overlap}(Y_{\text{sub}}, Y'), \quad (9)$$

where α weighs the two reward terms for "existence" and "overlap". Existence is 1 if any time point was correctly predicted within the labeled region, and 0 otherwise. The parameterized "overlap" function determines the finer properties of cardinality, size, and position. The cardinality parameter discounts the score if the prediction is an interrupted and fragmented range instead of being continuous. The overall size of the overlap of predicted and label ranges depends on a positional bias. It may favor "front", "middle", or "back" overlap. Practically, for some applications an early detection is preferable over a late detection.

Salient features outside of the labeled range Y_{sub_i} can be scored analogously, simply by inverting the range. For further details see Appendix A or Tatbul et al. (2018).

4. Experiments

Our evaluation compares visual interpretation methods on a set of network architectures and diverse classification datasets from the UCR repository, and on a more complex segmentation dataset. In total, we aggregate the results from 729 experiments. This section is divided into three parts. First, we discuss the metrics for the classification task (faithfulness, sensitivity, stability, robustness, sanity). Next, we investigate the influence of regularized model training on the faithfulness variants TS and TI and explain their differences. Finally, we discuss the new localization metric for the segmentation task. The code is available at <https://github.com/crispchris/saliency>.

4.1 Experimental Setup

We evaluate nine visual interpretation methods: Gradient (Simonyan et al., 2014), Integrated Gradient (Sundararajan et al., 2017), SmoothGrad (Smilkov et al., 2017), Guided Backpropagation (Springenberg et al., 2015), GradCAM (Selvaraju et al., 2017), Guided-GradCAM (Selvaraju et al., 2017), Layer-Wise Relevance Propagation (LRP) (Bach et al., 2015), LIME (Ribeiro et al., 2016), and Kernel SHAP (Lundberg and Lee, 2017). See Appendix B.2 for method-specific hyper-parameters.

For the classification tasks, we select the two commonly used model architectures Fully Convolutional Network (FCN) (Long et al., 2015) and Temporal Convolutional Network (TCN) (Bai et al., 2018). We do not focus on simpler architectures such as Multilayer Perceptrons and LSTMs (Hochreiter and Schmidhuber, 1997) due to noisy or vanishing saliency in preliminary studies. Our dataset selection follows related work (Fawaz et al., 2019b; Wang et al., 2017; Schlegel et al., 2019; Ates et al., 2021) that uses large, multivariate, multi-class datasets from diverse domains (GunPointAgeSpan, FordA, FordB, ElectricDevices, MelbournePedestrian, and NATOPS) from the UCR repository (Dau et al., 2018). We study faithfulness under the influence of dropout, ℓ_1 and ℓ_2 regularization separately with experiments that focus on the FCN and the datasets FordA, FordB and NATOPS. For the segmentation task, we consider two models: U-time (Perslev et al., 2019) (derived for time series from U-Net (Ronneberger et al., 2015)), and a bi-LSTM (Schuster and Paliwal, 1997). We provide details on each architecture in Appendix B.3. We evaluate them on the tool tracking (Löffler et al., 2021) dataset, a complex multivariate, multi-class time series from a 9-D magneto-inertial sensor, and use data from an electric screwdriver.

4.2 Evaluation on Classification Task

In this section, we discuss the six visual interpretation quality metrics for the classification task. Fig. 3 summarizes the scores for each metric over model architectures and datasets. Fig. 4 summarizes the scores for each metric over model architectures and methods.

Faithfulness. We evaluated both variants of faithfulness metrics and found significant differences. In general, methods are able to achieve higher scores in the Temporal Importance variant, compared to Temporal Sequence. This indicates that the visualiza-

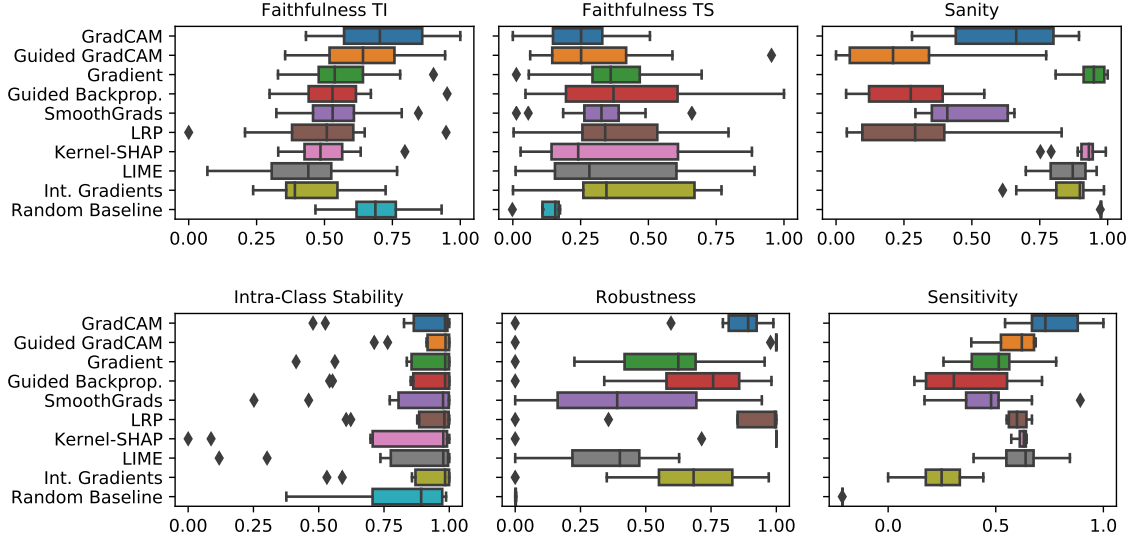


Figure 3: We aggregated results for TCN and FCN over all classification datasets {model architectures, datasets} without normalization (as we found that model architectures generally lead to similar scores).

tion methods are able to pinpoint individual features very faithfully, but fail to accurately capture dependencies on longer sequences. We also observe a relatively low correlation between methods - the visualizations that performed best in TI, i.e., GradCAM and Guided GradCAM, achieve only comparatively low scores in TS.

TS assumes that features are clustered and sequential. We hypothesize that this assumption is not valid for many time series domains. In particular, TS shows very low scores of low-variance for the FordA and NATOPS datasets in Fig. 4, which indicates that this assumption is potentially violated. Especially the multivariate NATOPS seems to exhibit diversely distributed features. For these reasons, we focus the following discussion on TI.

The TI scores of GradCAM and Guided GradCAM are above average, and Integrated Gradients below average. The more coarse GradCAM even slightly overtakes its Guided variant, likely due to GradCAM capturing the higher level features, and Guided-GradCAM’s sample-level interpolation introducing a bias. Integrated Gradients may fail due to the bias introduced by its user-defined baseline. The other methods perform similarly on average. The dataset centered view in Fig. 4 shows that the complex NATOPS dataset is the hardest to explain. This may be due to the potentially multi-dimensional features that are not perturbed.

Sanity. Across all datasets, we find that Gradient, Integrated Gradients, LIME, and Kernel-SHAP consistently achieve high sanity scores. In contrast, LRP, Guided GradCAM and Guided Backpropagation often assign similar saliency even after randomizing network parameters. This replicates sanity results by Adebayo et al. (2018). Low sanity methods highlight features in the input that may also be randomly extracted but do not necessarily predict classes.

Intra-class Stability. This metric is highly dependent on the dataset, e.g., centered samples as in GunPointAgeSpan. However, when accounting for variance introduced by the dataset (see Fig. 10b in Appendix C.2), SmoothGrads, LIME, and Kernel-SHAP show unstable saliency maps for the same classes. Not only the location in the sample, but also the warped distance between samples using DTW is different. Guided GradCAM is able to produce highly stable saliency maps across all datasets, likely due to its lower resolution.

It is important to notice that some datasets, e.g., FordA, do not necessarily have stable or similar features. However, many real datasets exhibit clearly stable features across classes, as evidenced through considerably higher scores for the ElectricDevices, GunPointAgeSpan, MelbournePedestrian, and NATOPS datasets. We found that a visual analysis of samples can be a useful indication for the inherent intra-class stability of a datasets - datasets with high scores exhibit relatively clear temporal features in specific orders, while those with low scores generally showed less localized features.

Methods that introduce additional biases into the visualization calculations, like Integrated Gradients and Guided GradCAM, can produce highly stable saliency maps. LIME and Kernel-SHAP look at individual sample points independently, and thus produce unstable saliency maps. We hypothesize that SmoothGrad’s addition of noise to sharpen the saliency maps can lead to an unintended side effect of over sharpening and overly focusing the saliency map onto a single, sample-local feature, that does not generalize to the rest of the dataset, which in turn leads to the low intra-class stability.

Robustness. Leaving aside the underlying model’s robustness, our evaluation of Gradient shows it is less robust, a finding that confirms Smilkov et al. (2017). Furthermore, LIME and, interestingly, SmoothGrads also show a low average robustness. The additive noise of SmoothGrads may compound and lead to diverging saliency maps. On the other hand, LRP, (Guided) GradCAM, and KernelSHAP show relatively robust saliency maps. Compared to purely gradient-based metrics, LRP and GradCAM use class activations, which might have a regularizing effect. Similarly, Kernel-SHAP can be thought of as a more constrained version of LIME. Overall, the saliency methods should capture the underlying model’s robustness and not produce saliency for divergent behavior, due to introduced biases. The robustness metric’s weakness is its computational cost: on {TCN,ElectricDevices} it reaches its time-out of 12 days.

Sensitivity. GradCAM shows the highest sensitivity for classes - the saliency maps for the most and least likely classes differ largely. On the other hand, Integrated Gradient and Guided Backpropagation produce similar saliency maps, independent of a sample’s class. This holds across all datasets. A possible explanation for this is that methods that introduce additional biases into the visualization calculations might lead to less sensitive saliency maps. Integrated Gradients integrates from a user-defined baseline. Guided Backpropagation intentionally suppresses the negative part of the gradient signals to find more visually focused and intuitive interpretations. While these biases can improve the visual appeal of the saliency maps, our results suggest that they have a not negligible impact on saliency maps and should be avoided when sensitivity is a concern.

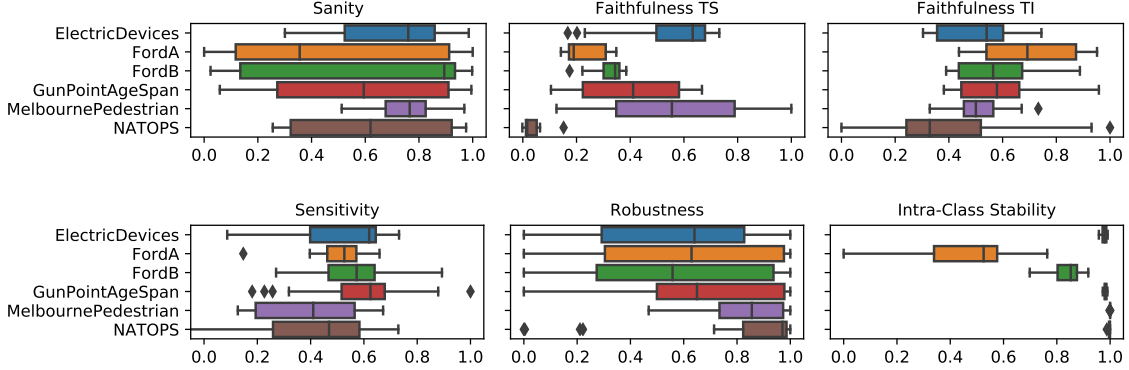


Figure 4: The plots show the influence of datasets on the scores, when we aggregate for each dataset over $\{\text{model architectures, methods}\}$. Similarity metrics for saliency maps yield different results in different domains.

4.3 Influence of Datasets and Models

First, datasets heavily impact scores, see the outliers in Fig. 3. The plots of the categories over each dataset for all $\{\text{model architectures, methods}\}$ in Fig. 4 emphasizes this finding. The choice of visual interpretation method depends, for the most part, on the task. Still, after normalizing for dataset bias, the relative scores do not diverge significantly but confirm the initial scores. We report the relative scores in Fig. 10b in Appendix C.2.

Surprisingly, the model architecture (FCN or TCN) only contributes little to the scores, see Fig. 10c in Appendix C.2. The scores for FCN and TCN diverge slightly more for faithfulness TS and TI. This may be due to the higher capacity of the TCN, which learns more diverse features, so that its TS score is lower and its TI score is higher. The FCN may learn fewer and less predictive features that are clustered more but are overall less predictive, resulting in higher TS score and lower TI score.

4.4 Influence of Regularization

Neural networks (among other parametric models) benefit from regularization techniques such as weight decay or dropout (Srivastava et al. (2014)). The positive effects can include increased accuracy and better generalization, essentially as a result of a decrease of overfitting to training data. However, we show that there are also unintended side effects of dropout, ℓ_1 and ℓ_2 regularization on the faithfulness of saliency methods, for which we give recommendations. We focus this section on an investigation of faithfulness, because other metrics only have an indirect relation to accuracy and thus regularization.

Hypotheses. We hypothesize differences in faithfulness due to regularization effects. *Dropout regularization* can be understood as computing the average of a number of thinned networks (Srivastava et al., 2014). Regularized models rely less on individual features. Hence, models should score higher in Temporal Importance, because of its arbitrary choice of input features of the highest saliency, and lower for Temporal Sequence that has a bias towards clusters of important features. Weight decay (Plaut et al., 1986), such as ℓ_1 or ℓ_2 regularization should result in the opposite learning effect. An ℓ_1 loss term causes sparsity

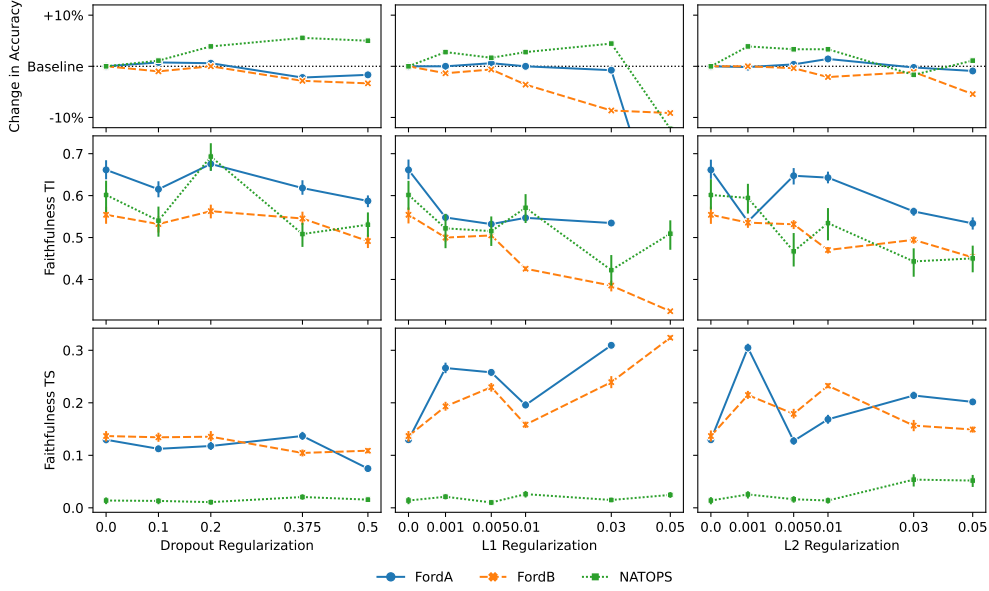


Figure 5: Accuracy (top), faithfulness TI (middle) and TS (bottom) scores for all visualizations across the FordA (blue), FordB (orange) and NATOPS (green) datasets.

of the parameters and supports finding the smallest required feature set. Models may learn fewer features, that in turn are of higher importance (Krogh and Hertz, 1991). This should result in higher scores for TS. More specifically, ℓ_2 regularization optimizes models to learn more features that are of similar importance, and thus equalize the importance of learned features (Plaut et al., 1986). Hence, their saliency’s faithfulness should perform similarly with the TI and TS variants.

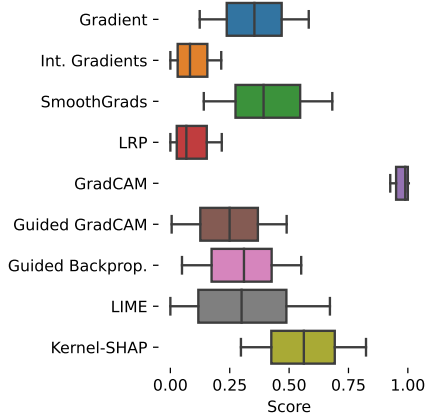
Accuracy. Fig. 5 shows how regularization impacts the accuracy of an FCN on FordA, FordB and NATOPS in the top row of plots. We show the relative change from the non-regularized baseline, indicated by with the hyper-parameter $\lambda = 0.0$, and average the results over two random seeds. Changes in accuracy vary between dropout, ℓ_1 and ℓ_2 and also between datasets. The accuracy on the FordA dataset is relatively stable with regularization, except for an outlier at the large ℓ_1 reg. of $\lambda = 0.05$. In contrast, the accuracy declines on FordB, with a downwards trend for increasing values of λ . Interestingly, the FCN benefits from regularization on the more complex NATOPS dataset. Dropout reliably improves accuracy, while the positive effect of weight decay is not as stable for larger λ of 0.05 (ℓ_1) and 0.03 (ℓ_2). The effect of a too large ℓ_1 weight decay is most detrimental, the model even fails to learn the two-class task FordA.

Absolute Faithfulness. We show the saliency methods’ aggregated Faithfulness TI and TS scores. Despite mostly similar accuracy for the regularization schemes, faithfulness scores differ strongly between them. For TI, a small dropout regularization produces better saliency than ℓ_1 or ℓ_2 regularization across all datasets, even though the accuracy for models is close, e.g., models for FordA perform within 1%. Interestingly, the opposite holds for

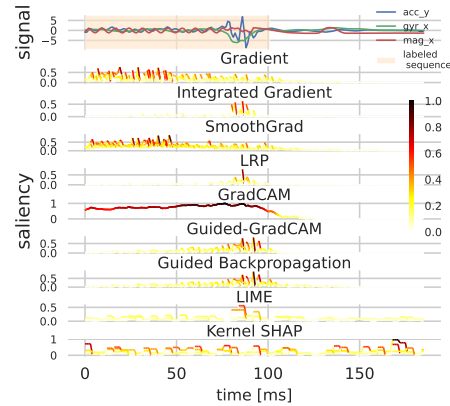
TS, where ℓ_2 regularization has a positive effect on the FordA and FordB datasets. ℓ_1 regularization displays a similar effect on all datasets. This confirms our hypotheses, that enforcing feature sparsity can have different effects on faithfulness TI and TS. We observe outliers for dropout regularization with $\lambda = 0.2$, that markedly improved faithfulness scores across datasets. A meaningful faithfulness score could not be computed for ℓ_1 regularization with $\lambda = 0.05$ on FordA, because the model did not exceed the performance of random guessing.

Accuracy and Faithfulness. Interestingly, we do not see that an increase in accuracy, e.g., for NATOPS or for ℓ_2 with $\lambda = 0.01$, consistently correlates with an increase in a TI score. This may be due to the limited fraction of input values (we use 20%) that we perturb while calculating TI. However, a decrease in accuracy tends to come with worse TI. Additionally to less accurate models, there may be a second effect at play. The thinning of features due to weight decay leads to fewer learned features. Perturbing less predictive features naturally results in lower TI scores. The FCN’s concentration on fewer features with ℓ_1 regularization is especially apparent in the Ford datasets’ trends in TS. This variant of faithfulness has a bias towards clustered features and benefits from feature sparsity.

We conclude from these experiments that regularization is important for both accuracy and faithful saliency. Any type of faithfulness directly depends on the relationship between accuracy of the models and saliency maps, even if it is not directly apparent when using a fixed fraction of perturbation when calculating TI, because regularization may increase or reduce feature sparsity in the model. Practitioners should choose a suitable regularization depending on the faithfulness variant. Similar test accuracy does not automatically imply similar faithfulness of saliency. This may be due to the numerical effects of weight decay and dropout on the networks’ parameters and feature learning.



(a) U-time localization with a "classic" bias.



(b) U-time examples.

Figure 6: Results for the localization metric on the tool tracking dataset and with all methods on U-time. We show detailed values for the localization metric in (a) and examples of saliency maps in (b).

4.5 Evaluation on Segmentation Task

This section presents the key findings from our evaluation when applying the localization metric on saliency maps generated from U-time (results for bi-LSTM are in Appendix C.1), trained for a segmentation task on the tool tracking dataset (Löffler et al., 2021). Fig. 6a shows the localization classical positional bias for each visualization method. Fig. 6b shows an exemplary saliency map for each method. Fig. 7 summarizes the statistics for the biases "classic", "front", "middle" and "back".

At first glance, GradCAM produces saliency maps with top scores in the localization metric. Additionally, its saliency maps appear much smoother and continuous, with high relevance located on the annotated segments. The high fidelity saliency map of Guided GradCAM instead produces lower scores due to its more nuanced relevancy assignments. This difference results from GradCAM’s coarser relevance, as its gradients do not flow to the input but stop at the last convolution layer. In contrast, LRP and Integrated Gradient produce lower scores. As Fig. 6b shows, the saliency maps highlight fewer relevant input features for the segmentation task, but instead features within the labeled sub-sequence that may be important for a classification.

Analysing the scores in Fig. 7 shows that saliency maps are located more in the "middle" of the annotated segments, compared to "front" and "back". This is also visible in the example in Fig. 6b where the relevance values start decreasing below the threshold of 0.5 already before the end of the labeled segment at 100 ms. This points towards a biased labeling process with longer sub-sequences assigned to the classes than necessary, and can hence help identifying faulty labels. Furthermore, the high variance of most results (except for GradCAM) shows that saliency maps for time series segmentation are noisy. This is especially the case for Kernel SHAP, where relevance is assigned seemingly at random.

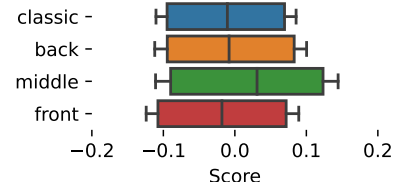


Figure 7: Localization biases for visualization methods on the tool tracking dataset.

GradCAM assigns saliency nearly perfectly to the labeled segments, compared to the other methods in this study that only marginally align with the annotated segments in the input features. Their saliency maps are comparatively noisy. However, each methods’ faithfulness has to be considered before choosing a saliency method to trust for producing interpretations, or even locating faulty labels or even spurious correlations. Interestingly, no method worked reliably on the bi-LSTM. We identify a lack of useful visualization methods for LSTMs, as CAM variants (GradCAM, Guided GradCAM, and Guided Backprop) are not applicable, see Fig. 9 in Appendix C.1 for detailed results.

In summary, localization scores of saliency for faithful models provide useful analysis of temporal biases and label inconsistencies, and can support the detection of shortcut learning. It is a red flag if an otherwise faithful saliency method has a low overlap of the saliency map and the potentially faulty label, or spurious correlations may be present. If saliency maps lie well within the labeled sub-sequence, but the saliency itself is not faithful, the score may hint at a bias present in the saliency method.

5. Recommendations

The quality of visualizations differs greatly between methods. No method passes the tests for all categories on all six datasets. This emphasizes the need to evaluate all metrics for every visual interpretation. We recommend to use a summary as in Fig. 8 to judge visualizations on every category, and propose the following guidelines for relative ranking. The absolute scores may be understood in comparison with a random baseline, similar to shuffled AUC (Borji et al., 2013).

Setup model training and regularization hyperparameters. As an initial step, we recommend to select a suitable set of regularization methods and their hyper parameters to optimize the models, depending on the task at hand. Dropout, ℓ_1 or ℓ_2 regularization may have a large effect on model’s inductive bias, and thus also on faithfulness. This also depends on the datasets’ feature distribution. Note that the right regularization can meaningfully improve the model interpretability, and we suggest changing parameters if objective metrics indicate a low trust in visualizations.

First: Ensure Faithfulness and Sanity. The general purpose of interpretability methods is to provide insights into model behavior. We propose to use the faithfulness and sanity scores to ascertain that a saliency map represents the model behavior. Faithfulness ensures that the saliency matches the model’s predictive features. Note that, depending on the prevalence of temporal correlations and sequential features in a dataset, an expert should choose between TS (when sequential features are important) and TI (when this is not the case). When in doubt, we propose to use TI.

Sanity checks confirm that saliency maps are sensitive to model parameters. This is important to avoid finding highly salient features, such as edges in images (Adebayo et al., 2018), while being insensitive to model parameters. We avoid saliency maps with low scores

Sanity	0.46	0.77	0.26	0.21	0.74	0.76	0.74	0.25	0.52	0.43
Faithfulness TS	0.35	0.54	0.52	0.54	0.42	0.09	0.47	0.58	0.42	0.49
Faithfulness TI	0.76	0.68	0.53	0.83	0.54	0.39	0.47	0.5	0.57	0.69
Sensitivity	0.98	0.84	0.57	0.66	0.34	0.66	0.68	0.67	0.45	0.99
Robustness	0.9	0.7	0.8	0.98	0.6	0.98	0.53	0.87	0.42	0.38
Intra-Class Stability	0.65	0.69	0.74	0.95	0.76	0.2	0.52	0.86	0	0.46
	GradCAM	Gradient	Guided Backprop.	Guided GradCAM	Int. Gradients	Kernel-SHAP	LIME	LRP	Random Baseline	SmoothGrads

Figure 8: Scores as a heatmap for TCN on FordB. Columns with high relative scores (bright squares) indicate good visualizations. Dark squares show the shortcomings.

in either metric, as they do not reflect the model behavior. See Fig. 8 for an example: Gradient, Integrated Gradients, and LIME achieve the three highest-ranked scores. However, *random saliency maps* (second to the last column) are dissimilar (hence they also show high sanity scores) and their relatively high TI score of 0.57 hints that the faithfulness of the other methods is not completely reliable and additional tests are required. Guided Backprop, Guided GradCAM and LRP fail the sanity check, while Kernel-SHAP performs poorly in faithfulness.

Second: Check Sensitivity and Robustness. Once faithfulness and sanity are established, we propose to look at sensitivity and robustness of the generated saliency maps. A low inter-class sensitivity can indicate that the saliency maps only focus on the predicted class and underestimate the importance of features that do not belong to this class. A low robustness score suggests that the visualization method is susceptible to adversarial examples and small perturbations in the input. Given that the model predictions are robust (Zhang et al., 2019), and the saliency is faithful, a low robustness implies that the saliency method cannot be trusted, and may even be manipulated (Dombrowski et al., 2019). For non-robust models we recommend to rely less on visual interpretations, especially if they have low faithfulness. According to Fig. 8, we keep Gradient and LIME, but disregard Integrated Gradients due to its lower sensitivity.

Detailed Analysis: Analyze Intra-class Stability and Localization. Intra-class stability measures how much saliency maps for one class agree between different samples. The localization metric, like other Pointing Game-like metrics, measures semantic precision based on annotations. They allow experts to choose and analyze saliency methods that are more intuitive and understandable. Note that it is crucial to ensure the faithfulness of a method before relying on this metric. If the method is not faithful, then stable and localized visualizations are visually pleasing, but do not reflect model behavior. This can hide issues like spurious correlations (Arjovsky et al., 2019) or the shortcut learning problem (Geirhos et al., 2020) behind a higher score.

6. Conclusion

We propose an evaluation scheme for visual interpretations on time series data and provide extensive empirical results for different visualizations, models, datasets, and regularization methods across time series classification and segmentation. We recommend six orthogonal metrics that provide a disentangled evaluation of important characteristics of visual interpretations. All these metrics should be evaluated for every visual interpretation to prevent relying on interesting but spurious results. We also show how each perspective evaluates different strengths and weaknesses of visualization methods, and give recommendations on their use. The main findings are:

- No individual visualization method achieves high scores on all evaluation methods. For practitioners, we thus recommend to focus on faithfulness (TI) and sanity first.
- The strong impact of datasets onto the saliency methods was consistent across all evaluation perspectives. This indicates that the interpretability of the underlying model is similarly dependent on the learned distribution as its predictive accuracy.
- Similarly, visual interpretation methods may introduce an additional bias into the visualization calculations. We show that this can lead to highly stable saliency maps.

- Regularization during training had a large, but inconsistent influence on faithfulness. High regularization tends to decrease TI, but increase the TS variant.
- Model architecture of convolutional networks alone had a relatively low impact on evaluation scores for visualization methods, compared to MLP or LSTM, that were noisy or suffered from vanishing saliency.
- Our novel localization metric for segmentation analyzes if saliency is assigned correctly to local features and help to evaluate label ranges. GradCAM displays an outstanding localization of features, surpassing other methods.

Overall, our work demonstrates how the explanations of state-of-the-art visualization methods differ wildly. Using faithfulness and sanity scores, experts can distinguish between plausible but wrong saliency maps. Since visualization methods are used to explain neural networks to human experts, more quality measures are necessary. Explanations need to be sensitive for classes, robust (if the model is robust) and stable (if model operation is consistent), while staying true to the model behavior. We combine these requirements into a simple and clear framework that can be used to assess visual interpretations on time series data for arbitrary neural networks.

Future work investigates the relatively high scores of the random baseline in the two main metrics sanity and faithfulness. Furthermore, our study of regularization shows that model training should be optimized for more reliable interpretability, so that they behave more intuitively, without sacrificing predictive performance. Finally, the localization metric may be adapted to detect spurious correlations in time series problems.

REPRODUCIBILITY

This paper includes supplemental materials to improve reproducibility. Most importantly, we publish the code for model training and dataset loaders, for generating visual interpretations and of all evaluation metrics. Furthermore, all datasets are publicly available.

Acknowledgments

We would like to acknowledge support for this project from the Bavarian Ministry of Economic Affairs, Infrastructure, Energy and Technology as part of the Bavarian project Leistungszentrum Elektroniksysteme (LZE) and the Center for Analytics-Data-Applications (ADA-Center) within the framework of “BAYERN DIGITAL II”.

Appendix A.

A. Localization Metric Positional Biases

This section explains the "existence" and "overlap" terms of our localization metric. Note again the recall score as

$$S_{\text{recall}}(Y_{\text{sub}}, Y') = \alpha \cdot \text{existence}(Y_{\text{sub}}, Y') + (1 - \alpha) \cdot \text{overlap}(Y_{\text{sub}}, Y'), \quad (10)$$

The "existence" and "overlap" terms are defined by Tatbul et al. (2018) as follows. First, existence is defined as a correct prediction of one sample point at index j of the correct class within the labeled region:

$$\text{existence}(Y_{\text{sub}}, Y') = \begin{cases} 1, & \text{if } \sum_{j=1}^{|Y'|} |Y_{\text{sub}} \cap Y'_j| \geq 1 \\ 0, & \text{otherwise} \end{cases} \quad (11)$$

The overlap determines the finer properties cardinality $\gamma()$, size $\omega()$ and position $\delta()$.

$$\text{overlap}(Y_{\text{sub}}, Y') = \text{cardinality}(Y_{\text{sub}}, Y') \cdot \sum_{j=1}^T \omega(Y_{\text{sub}}, Y_{\text{sub}} \cap Y'_j, \delta) \quad (12)$$

$$\text{cardinality}(Y_{\text{sub}}, Y') = \begin{cases} 1, & \text{if } Y_{\text{sub}} \text{ overlaps with at most one } Y'_j \in Y' \\ \gamma(Y_{\text{sub}}, Y'), & \text{otherwise} \end{cases} \quad (13)$$

The term α ($0 \leq \alpha \leq 1$) weights existence and the following qualitative measures of overlap. The three user-defined functions return values of $0 \leq \gamma() \leq 1$, $0 \leq \omega() \leq 1$ and $\delta() \geq 1$. The cardinality $\gamma()$ function weighs the prediction of a continuous range Y' covering the whole labeled range Y_{sub} versus interrupted ranges in a fragment manner. The overall size $\omega()$ of the agreement of predicted and label ranges depends on the positional bias $\delta()$ and can favor "front", "middle", or "back". Practically, for some applications an early detection is preferable to a late detection. For the four functions, we selected α is equal to 0, γ is equal to 1. ω depends on the position bias δ and for δ we have three variants, "front", "middle" or "back", proposed by Tatbul et al. (2018).

B. Experimental Setup

We describe each visual interpretation method shortly in Sec. B.1, then the hyper parameters for each visual interpretation method in Sec. B.2 and for the optimizer and networks in Sec. B.3.

B.1 Categorization of Methods

This Section provides a short introduction to the methods that we use in our experiments.

Gradient-based methods. Gradient (Simonyan et al., 2014) computes class c 's saliency map M^c using the derivative of the class score P^c of model with respect to the input sample x , as $M^c(x) = \frac{\partial P^c}{\partial x}$. However, Gradient suffers from the *saturation problem* (a feature may have global importance, but its local derivative is small (Smilkov et al., 2017)), local sensitivity, and noisy saliency maps (due to (sharp) local variations in the gradients (Smilkov et al., 2017)). Follow-up work smooths the gradients to reduce noise (Smilkov et al., 2017), applies special propagation rules instead of propagating a gradient (Arras et al., 2017), or propagates only up to a specific intermediate layer (Selvaraju et al., 2017).

Perturbation-based methods. Ribeiro et al. (2016) proposed Local Interpretable Model-Agnostic Explanations (LIME), that fits a local surrogate model (e.g., a linear regression) as an explanation and uses this surrogate to calculate relevance. Kernel SHAP (Lundberg and Lee, 2017) builds on LIME, but calculates Shapley values that measure the contribution of individual features to the input more accurately.

B.2 Visualization Methods Hyper Parameters

We set the hyper parameters for each visual interpretation method according to their recommendations from literature. We provide the reasoning behind the selected parameters in the following paragraphs.

Gradient computes the derivative of the target class score with respect to the input sample and returns the saliency map of the input sample at the end. Integrated Gradient uses the linear path method to compute gradient along the path from a baseline x' . We use a zero vector for the baseline. As suggested by Smilkov et al. (2017), the number of steps for the path should be selected between 20 and 300. Hence, we use steps $N = 60$, meaning that it takes 60 steps from baseline x' to the original input sample x , according to $x = x' + \frac{(x-x')}{N} \cdot n$, n is the current step.

SmoothGrad also computes the derivative of the target class score with respect to the input sample. However, it adds Gaussian noise $\mathcal{N}(0, \sigma^2)$ to the input sample multiple times and computes the gradients from the perturbed samples ($x + \mathcal{N}(0, \sigma^2)$). The number of iteration of adding noise is chosen $N = 60$ and the standard deviation of Gaussian noise is chosen $\sigma = 0.2$.

For LRP, we select the ϵ -propagation rule for every DL model with $\epsilon = 1e - 9$. Due to the residual block in TCN model the propagated relevances should therefore be added together ($R = R_1 + R_2$).

GradCAM and Guided-GradCAM are designed for models with convolutional layers, i.e. FCN, TCN and U-time. GradCAM focuses on the last convolutional layer, which produces feature maps, whose shapes usually are smaller than the shape of input samples. Therefore, we use interpolation to up-sample the saliency maps from the last convolution layer to match their shape to the shape of the input samples, which allows us to visualize them in the input space. Because of ReLU functions, GradCAM returns only positive relevances.

For LIME, we use the cosine distance function as the kernel function with width $w = 5.0$ to weight the perturbed samples, and perform 1000 iterations. For the perturbation, we consider that neighbors along time dimension should have similar relevance to reduce the computational time, so we set the number of features along time dimension 50 for GunPointAgeSpan. This means that saliency maps for samples with length 150 in Gun-

PointAgeSpan have same relevance for every 3 neighbors and saliency maps for dense labeling samples in tool tracking have same relevance for every 4 neighbors.

For Kernel SHAP, we use 1000 iterations and set the number of features along time dimension to 50. Furthermore, the sampling of feature perturbation in Kernel SHAP is based on the distribution $p(f) = \frac{(F-1)}{(f \cdot (F-f))}$, where f is the number of selected features and F is the total number of features in interpretation space.

B.3 Network Architectures

We use the Adam optimizer with a learning rate of 0.002. We train every dataset for 600 epochs (with early stopping after 80 epochs). We use a Cross Entropy loss for time series classification and a Generalized Dice loss with Cross Entropy function for time series segmentation.

For the time series segmentation task on the tool tracking dataset, we report an accuracy of 83% for U-time and 85% for the bi-LSTM. Table 1 shows the classification results for FCN and TCN with all classification datasets.

datasets	model architectures	
	FCN	TCN
GunPointAgeSpan	88.38 ± 2.44	95.91 ± 2.27
FordA	89.43 ± 0.31	91.42 ± 0.35
FordB	75.47 ± 1.71	79.38 ± 1.31
MelbournePedestrian	90.94 ± 0.98	88.39 ± 5.23
NATOPS	95.79 ± 1.56	90.0 ± 7.09
ElectricDevices	67.49 ± 2.44	68.0 ± 1.96

Table 1: The test accuracy in % of the classification task.

B.3.1 FULLY CONVOLUTION NETWORK

We use a slightly modified FCN, similar to Wang et al. (2017). Ours contains four convolution blocks with a convolutional layer, a batch normalization layer (Ioffe and Szegedy, 2015) and a ReLU layer in each block. The kernel shapes and numbers of filter for convolution layers are $\{7, 5, 3, 3\}$ and $\{16, 32, 32, 16\}$. Therefore, there are four convolutional layers. Each convolutional layer has unit stride and no padding, which means the time sequence will be reduced continuously by the blocks. The final convolution block, which is behind the four convolution blocks, does not have a ReLU layer and contains a 1×1 convolutional layer. The 1×1 convolutional layer serves as a projection layer. It can not only reduce the channel size of feature maps but also keep their salient features. Finally, we apply Global Max Pooling on the features maps, before the softmax operation.

B.3.2 TEMPORAL CONVOLUTION NETWORK

For the TCN, that was first proposed by (Bai et al., 2018), we use a global pooling layer for the prediction. In our architecture, TCN has the convolution filters $\{16, 32, 32, 32\}$ and

kernel shapes for convolution layers $\{7, 5, 5, 5\}$ in four residual blocks. Therefore, the total number of layers is 8.

B.3.3 BIDIRECTIONAL LONG SHORT-TERM MEMORY

We use a standard, single-layer bi-LSTM to predict dense labels for the segmentation task, as implemented in PyTorch, with 512 hidden units. There is a dense layer behind the LSTM model to fit the hidden units 512 to the number of classes. Also, the dropout rate is set to 0.2 to prevent overfitting.

B.3.4 U-TIME

We use the U-time (Perslev et al., 2019) architecture with the following configuration. In each convolution block, there are two dilated convolution layers with dilation 3, followed by a ReLU layer, a batch normalization layer, and a Max-Pooling layer at the end. The number of filters for convolution layers in four convolution blocks are $\{16, 32, 64, 128\}$ and the pooling window sizes are all 2. Two additional convolutions with filter numbers $\{256, 256\}$ follow after four convolution blocks. In each transposed convolution block, a nearest-neighbor up-sampling (Odena et al., 2016) of its input is implemented, followed by a dilated convolution layer with dilation 3, a ReLU layer and a batch normalization layer. The number of filters for convolution layers in four transposed convolution blocks are in the reverse order of the encoder $\{128, 64, 32, 16\}$. The kernel size of convolution layers in both encoder and decoder is 7.

C. Additional results

We report additional results to supplement our discussion for a bi-LSTM architecture on the segmentation task in Sec. C.1, and for the classification task in Sec. C.2.

C.1 Evaluation on Segmentation Task: bi-LSTM

The results for bi-LSTM on the segmentation task for tool tracking in Fig. 9 show that none of the visual interpretation methods, that are compatible with the model’s architecture, produce satisfactory saliency maps.

C.2 Classification Task

We show the variability of each visualization method with respect to each dataset and metric category for the TCN in Fig. 10a. It is noteworthy that some datasets are more problematic for the methods, especially for faithfulness and intra-class stability, than others. We also show that the model has only a small influence. For this result, we aggregate all datasets and visualization methods separately for FCN and TCN in Fig. 10c.

In order to compare methods independent of datasets, we control for their bias by normalizing the scores of all methods for each $\{\text{category}, \text{dataset}\}$ so that their mean is 0 and variance is 1. With this, we can correctly assess the "relative" performance of the visual interpretation methods across different datasets. The plot in Fig. 10b shows these

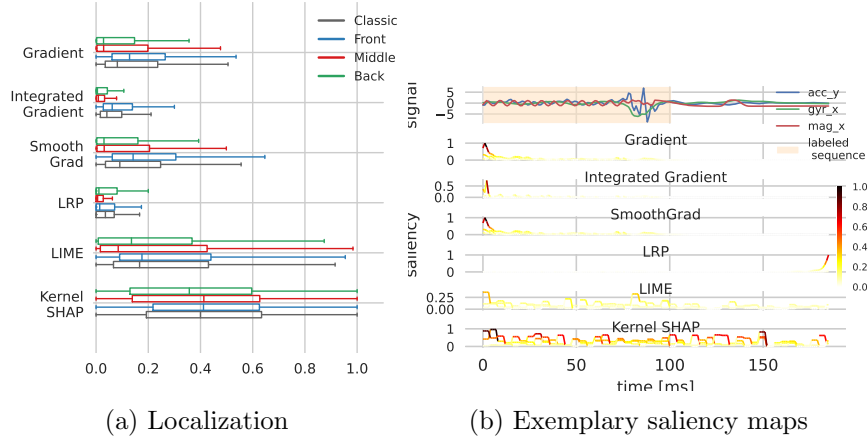
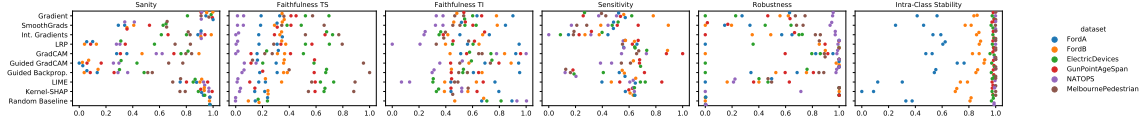


Figure 9: We show the localization metric results for all methods on the tool tracking dataset and with the bi-LSTM model. (a) shows the results for the localization metric. (b) shows exemplary saliency maps.

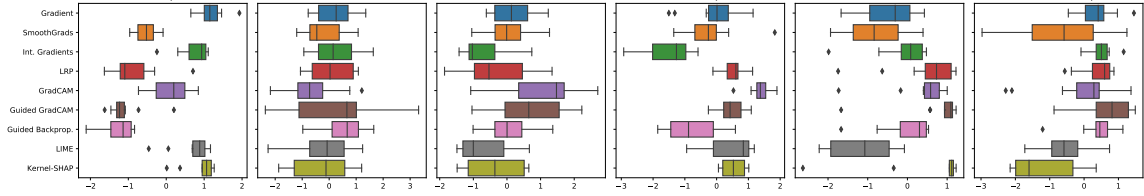
relative (or marginal) scores that a method can achieve, compared to other methods on the same datasets.

We prove the orthogonality of metrics in Figure 11. No combination of our metric scores shows a high correlation. This shows that each metric measures a quality independent of all other metrics.

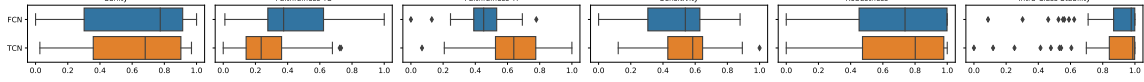
We show examples for saliency of the TCN architecture on the FordB dataset for the visual interpretation methods for class 0 in Figure 12 and class 1 in Figure 13. We argue that the choice of a suitable method to generate saliency maps should be guided by our framework.



(a) Separated datasets.



(b) Relative scores that a method can achieve compared to other methods on the same datasets.



(c) Results for different model architectures, aggregated across datasets and visual interpretability methods. Model architecture has a comparatively small influence on the performance, which speaks to their generalization capabilities.

Figure 10: (a) shows scores separately over all $\{\text{model, method}\}$ combinations. (b) removes the datasets' bias in order to assess the performance of individual visual interpretability metrics independent from datasets. (c) shows results for different model architectures, aggregated across datasets and visual interpretability methods. Model architecture has a comparatively small influence on the performance, which speaks to their generalization capabilities.

References

- J. Adebayo, J. Gilmer, M. Muelly, I. Goodfellow, M. Hardt, and B. Kim. Sanity checks for saliency maps. In *Advances in Neural Information Processing Systems*, 2018.
- D. Alvarez Melis and T. Jaakkola. Towards robust interpretability with self-explaining neural networks. In *Advances in Neural Information Processing Systems*, 2018.
- D. Alvarez-Melis and T. S. Jaakkola. On the robustness of interpretability methods. In *Proceedings of the 2018 ICML Workshop in Human Interpretability in Machine Learning*, Stockholm, Sweden, 2018.
- M. Ancona, E. Ceolini, C. Öztireli, and M. Gross. Towards better understanding of gradient-based attribution methods for deep neural networks. In *International Conference on Learning Representations*, 2018.
- M. Arjovsky, L. Bottou, I. Gulrajani, and D. Lopez-Paz. Invariant risk minimization. *arXiv preprint arXiv:1907.02893*, 2019.
- L. Arras, G. Montavon, K.-R. Müller, and W. Samek. Explaining recurrent neural network predictions in sentiment analysis. In *Proceedings of the 8th Workshop on Computational*

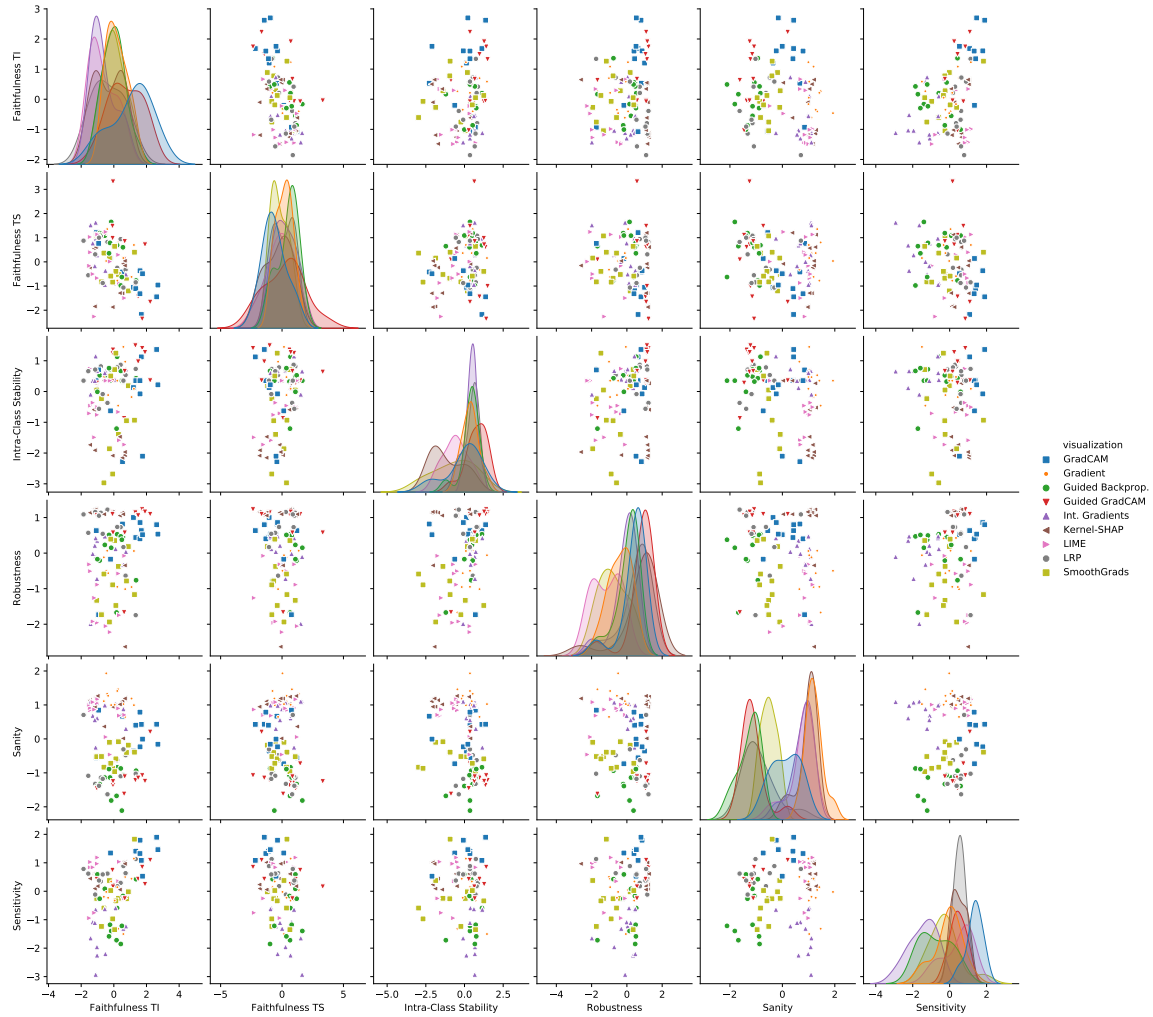


Figure 11: Pairplots of the correlations of metric scores with each other. No combination of metrics has a meaningful correlation with each other, proving that they provide independently useful signals. This analysis is based on scores that were normalized for dataset bias, but the results also hold when this normalization is not done.

Approaches to Subjectivity, Sentiment and Social Media Analysis, pages 159–168, Copenhagen, Denmark, Sept. 2017.

A. B. Arrieta, N. Díaz-Rodríguez, J. Del Ser, A. Bennetot, S. Tabik, A. Barbado, S. García, S. Gil-López, D. Molina, R. Benjamins, et al. Explainable artificial intelligence (xai): Concepts, taxonomies, opportunities and challenges toward responsible ai. *Information Fusion*, 58:82–115, 2020.

E. Ates, B. Aksar, V. J. Leung, and A. K. Coskun. Counterfactual explanations for multivariate time series. In *2021 International Conference on Applied Artificial Intelligence (ICAPAI)*, pages 1–8, Halden, Norway, May 2021.

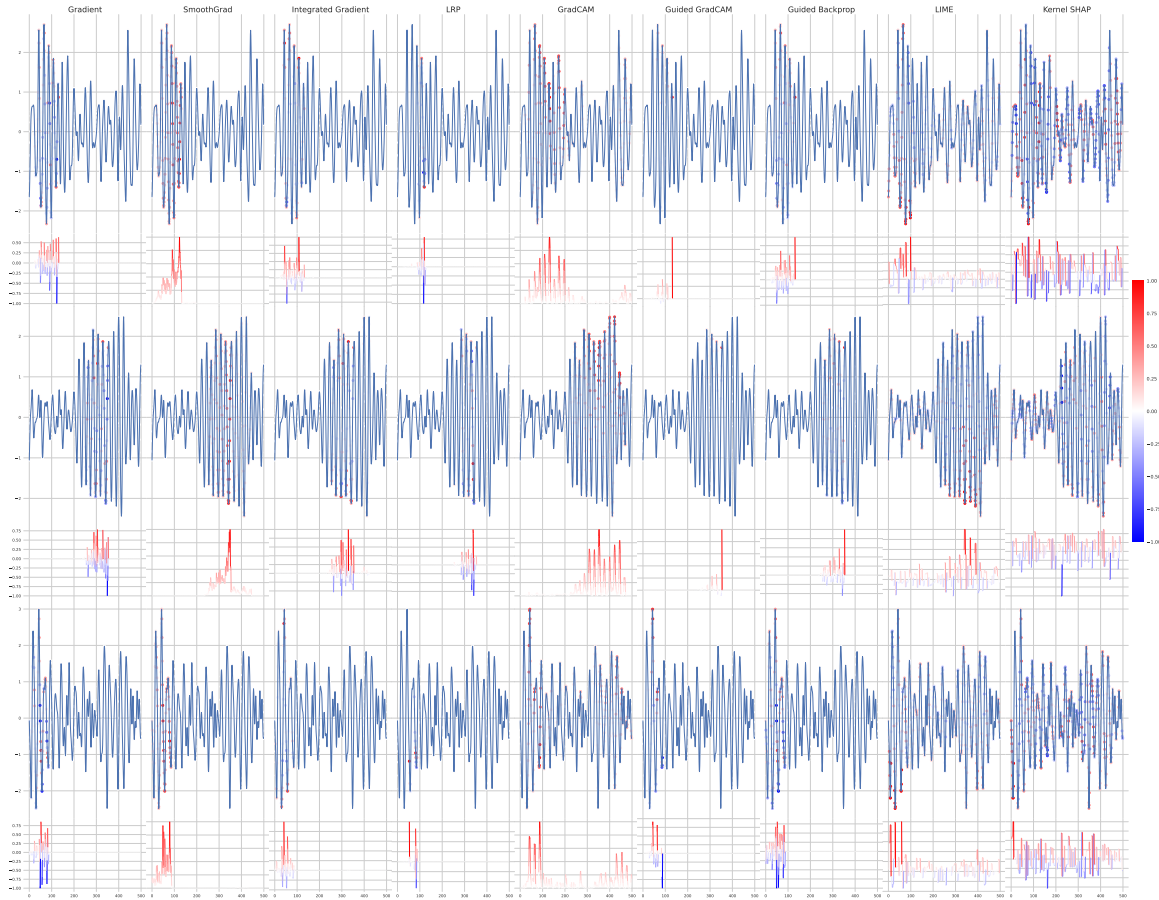


Figure 12: Examples of saliency maps for the TCN architecture on the FordB dataset for class 0.

S. Bach, A. Binder, G. Montavon, F. Klauschen, K.-R. Müller, and W. Samek. On pixel-wise explanations for non-linear classifier decisions by layer-wise relevance propagation. *PLOS ONE*, 10(7):1–46, 07 2015. doi: 10.1371/journal.pone.0130140.

S. Bai, J. Z. Kolter, and V. Koltun. An empirical evaluation of generic convolutional and recurrent networks for sequence modeling. *arXiv preprint arXiv:1803.01271*, 2018.

F. Berkenkamp, M. Turchetta, A. P. Schoellig, and A. Krause. Safe model-based reinforcement learning with stability guarantees. In *Proc. of the 31st Intl. Conf. on Neural Information Processing Systems*, page 908–919, 2017.

A. Borji, H. R. Tavakoli, D. N. Sihite, and L. Itti. Analysis of scores, datasets, and models in visual saliency prediction. In *Proceedings of the IEEE International Conference on Computer Vision (ICCV)*, December 2013.

D. V. Carvalho, E. M. Pereira, and J. S. Cardoso. Machine learning interpretability: A survey on methods and metrics. *Electronics*, 8(8):832, Jul 2019. ISSN 2079-9292.

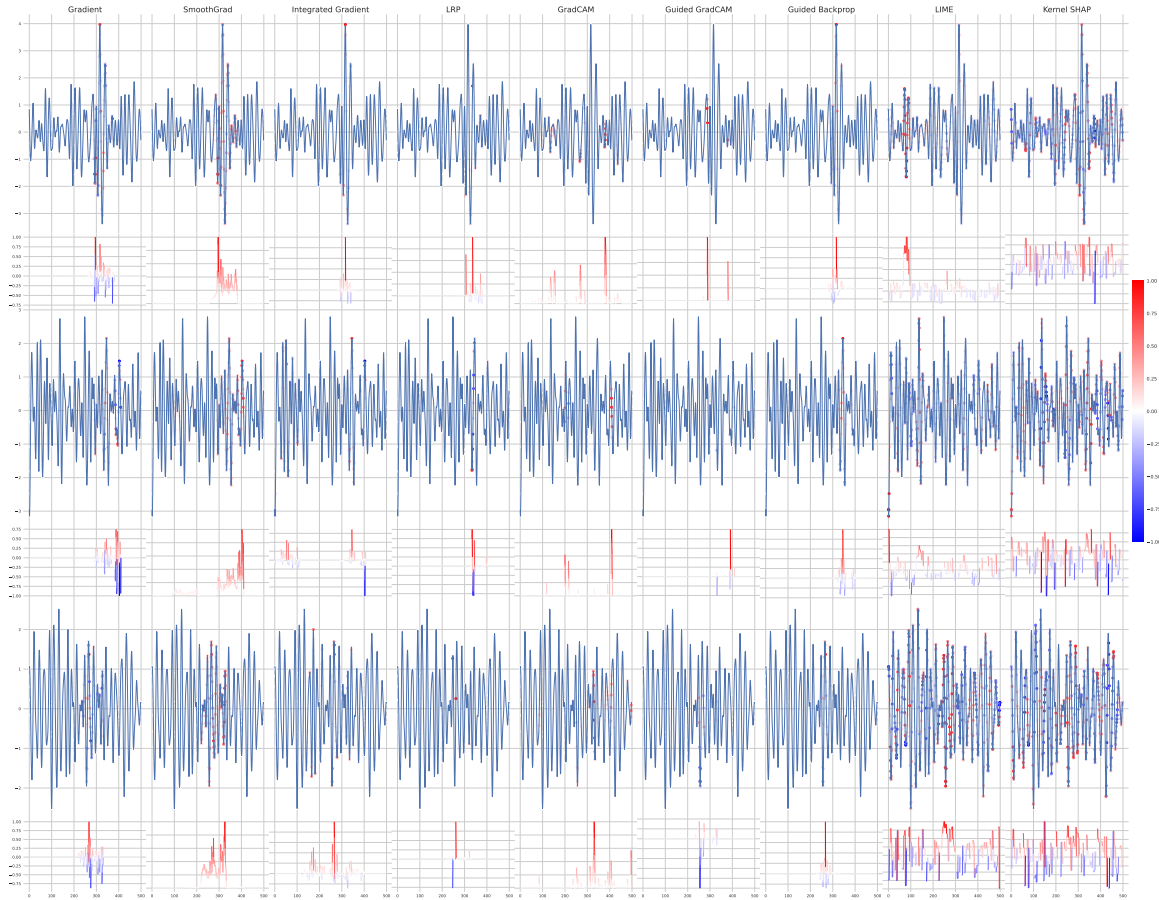


Figure 13: Examples of saliency maps for the TCN architecture on the FordB dataset for class 1.

H. Dau, A. Bagnall, K. Kamgar, M. Yeh, Y. Zhu, S. Gharghabi, and C. Ratanamahatana. The UCR time series archive. *ArXiv e-prints*, arXiv:1810.07758, 2018.

A.-K. Dombrowski, M. Alber, C. Anders, M. Ackermann, K.-R. Müller, and P. Kessel. Explanations can be manipulated and geometry is to blame. In H. Wallach, H. Larochelle, A. Beygelzimer, F. d'Alché-Buc, E. Fox, and R. Garnett, editors, *Advances in Neural Information Processing Systems*, volume 32, 2019.

E. Dorschky, M. Nitschke, C. Martindale, A. J. van den Bogert, A. Koelewijn, and B. Eskofier. CNN-Based Estimation of Sagittal Plane Walking and Running Biomechanics From Measured and Simulated Inertial Sensor Data. *Frontiers in Bioengineering and Biotechnology*, 8:1–14, 2020.

F. Doshi-Velez and B. Kim. Towards a rigorous science of interpretable machine learning. *arXiv preprint arXiv:1702.08608*, 2017.

H. I. Fawaz, G. Forestier, J. Weber, L. Idoumghar, and P.-A. Muller. Accurate and interpretable evaluation of surgical skills from kinematic data using fully convolutional neural

- networks. *International Journal of Computer Assisted Radiology and Surgery*, 14:1611 – 1617, 2019a.
- I. H. Fawaz, G. Forestier, J. Weber, L. Idoumghar, and P.-A. Muller. Deep learning for time series classification: a review. *Data Mining and Knowledge Discovery*, 33, 07 2019b.
- T. Fel and D. Vigouroux. Representativity and consistency measures for deep neural network explanations. *arXiv preprint arXiv:2009.04521*, 2020.
- R. Geirhos, J.-H. Jacobsen, C. Michaelis, R. Zemel, W. Brendel, M. Bethge, and F. A. Wichmann. Shortcut learning in deep neural networks. *Nature Machine Intelligence*, 2 (11):665–673, 2020.
- B. Goodman and S. Flaxman. European union regulations on algorithmic decision-making and a “right to explanation”. *AI magazine*, 38(3):50–57, 2017.
- J. Han, M. Kamber, and J. Pei. 2 - getting to know your data. In *Data Mining (Third Edition)*, The Morgan Kaufmann Series in Data Management Systems, pages 39–82. Boston, 2012.
- S. Hochreiter and J. Schmidhuber. Long short-term memory. *Neural Computation*, 9(8): 1735–1780, 1997.
- S. Ioffe and C. Szegedy. Batch normalization: Accelerating deep network training by reducing internal covariate shift. In *Proc. of the 32nd Intl. Conf. on Machine Learning*, page 448–456, 2015.
- A. A. Ismail, M. Gunady, H. Corrada Bravo, and S. Feizi. Benchmarking deep learning interpretability in time series predictions. In *Advances in Neural Information Processing Systems*, volume 33, pages 6441–6452, 2020.
- Z. Jianming, L. Zhe, B. Jonathan, S. Xiaohui, and S. Stan. Top-down neural attention by excitation backprop. In *European Conference on Computer Vision(ECCV)*, 2016.
- A. Krogh and J. Hertz. A simple weight decay can improve generalization. *Advances in neural information processing systems*, 4, 1991.
- X.-H. Li, Y. Shi, H. Li, W. Bai, C. C. Cao, and L. Chen. An experimental study of quantitative evaluations on saliency methods. In *Proceedings of the 27th ACM SIGKDD Conference on Knowledge Discovery & Data Mining*, pages 3200–3208, 2021.
- C. Löffler, C. Nickel, C. Sobel, D. Dzibela, J. Braat, B. Gruhler, P. Woller, N. Witt, and C. Mutschler. Automated quality assurance for hand-held tools via embedded classification and automl. In *Machine Learning and Knowledge Discovery in Databases. Applied Data Science and Demo Track*, pages 532–535, 2021.
- J. Long, E. Shelhamer, and T. Darrell. Fully convolutional networks for semantic segmentation. In *Proceedings of the IEEE conference on computer vision and pattern recognition*, pages 3431–3440, 2015.

- S. M. Lundberg and S.-I. Lee. A unified approach to interpreting model predictions. In *Advances in Neural Information Processing Systems*, volume 30, 2017.
- A. Odena, V. Dumoulin, and C. Olah. Deconvolution and checkerboard artifacts. *Distill*, 1(10):e3, 2016.
- F. Oviedo, Z. Ren, S. Sun, C. Settens, Z. Liu, N. T. P. Hartono, S. Ramasamy, B. L. DeCost, S. I. Tian, G. Romano, et al. Fast and interpretable classification of small x-ray diffraction datasets using data augmentation and deep neural networks. *npj Computational Materials*, 5(1):1–9, 2019.
- M. Perslev, M. Jensen, S. Darkner, P. J. r. Jennum, and C. Igel. U-time: A fully convolutional network for time series segmentation applied to sleep staging. In *Advances in Neural Information Processing Systems 32*, pages 4415–4426. Curran Associates, Inc., 2019.
- D. C. Plaut, S. J. Nowlan, , and G. E. Hinton. Experiments on learning by back propagation. *Technical report, Carnegie-Mellon Univ., Pittsburgh, Pa. Dept. of Computer Science.*, 1986.
- S.-A. Rebuffi, R. Fong, X. Ji, and A. Vedaldi. There and back again: Revisiting backpropagation saliency methods. In *Conference on Computer Vision and Pattern Recognition (CVPR)*, 2020.
- M. T. Ribeiro, S. Singh, and C. Guestrin. “why should i trust you?”: Explaining the predictions of any classifier. In *Proc. of the 22nd ACM SIGKDD Intl. Conf. on Knowledge Discovery and Data Mining*, page 1135–1144, 2016.
- T. Rojat, R. Puget, D. Filliat, J. Del Ser, R. Gelin, and N. Díaz-Rodríguez. Explainable artificial intelligence (xai) on timeseries data: A survey. *arXiv preprint arXiv:2104.00950*, 2021.
- O. Ronneberger, P. Fischer, and T. Brox. U-net: Convolutional networks for biomedical image segmentation. In *Medical Image Computing and Computer-Assisted Intervention (MICCAI)*, volume 9351 of *LNCS*, pages 234–241. Springer, 2015.
- W. Samek, A. Binder, G. Montavon, S. Lapuschkin, and K.-R. Müller. Evaluating the visualization of what a deep neural network has learned. *IEEE Transactions on Neural Networks and Learning Systems*, 28:2660–2673, 11 2017. doi: 10.1109/TNNLS.2016.2599820.
- W. Samek, G. Montavon, S. Lapuschkin, C. J. Anders, and K.-R. Müller. Explaining deep neural networks and beyond: A review of methods and applications. *Proc. of the IEEE*, 109(3):247–278, 2021.
- U. Schlegel, H. Arnout, M. El-Assady, D. Oelke, and D. Keim. Towards a rigorous evaluation of xai methods on time series. *IEEE/CVF Intl. Conf. on Computer Vision Workshop (ICCVW)*, pages 4197–4201, 2019.

- L. M. Schmidt, G. Kontes, A. Plinge, and C. Mutschler. Can you trust your autonomous car? interpretable and verifiably safe reinforcement learning. In *IEEE Intelligent Vehicles Symposium (IV)*, pages 171–178, 2021.
- M. Schuster and K. Paliwal. Bidirectional recurrent neural networks. *IEEE Transactions on Signal Processing*, 45(11):2673–2681, 1997.
- R. R. Selvaraju, M. Cogswell, A. Das, R. Vedantam, D. Parikh, and D. Batra. Grad-cam: Visual explanations from deep networks via gradient-based localization. In *IEEE Intl. Conf. on Computer Vision*, pages 618–626, 2017.
- K. Simonyan, A. Vedaldi, and A. Zisserman. Deep inside convolutional networks: Visualising image classification models and saliency maps. *arXiv preprint arXiv:1312.6034*, 2014.
- D. Smilkov, N. Thorat, B. Kim, F. Viégas, and M. Wattenberg. Smoothgrad: removing noise by adding noise. *arXiv preprint arXiv:1706.03825*, 2017.
- J. T. Springenberg, A. Dosovitskiy, T. Brox, and M. A. Riedmiller. Striving for simplicity: The all convolutional net. In Y. Bengio and Y. LeCun, editors, *3rd International Conference on Learning Representations, ICLR 2015*, 2015.
- N. Srivastava, G. Hinton, A. Krizhevsky, I. Sutskever, and R. Salakhutdinov. Dropout: A simple way to prevent neural networks from overfitting. *J. Mach. Learn. Res.*, 15(1):1929–1958, Jan. 2014. ISSN 1532-4435.
- N. Strodthoff and C. Strodthoff. Detecting and interpreting myocardial infarction using fully convolutional neural networks. *Physiological Measurement*, 40(1):015001, jan 2019.
- M. Sundararajan, A. Taly, and Q. Yan. Axiomatic attribution for deep networks. In *International Conference on Machine Learning*, pages 3319–3328. PMLR, 2017.
- N. Tatbul, T. J. Lee, S. Zdonik, M. Alam, and J. Gottschlich. Precision and recall for time series. In *Advances in Neural Information Processing Systems*, volume 31, 2018.
- T. K. Vintsyuk. Speech discrimination by dynamic programming. *Cybernetics*, 4(1):52–57, 1968.
- Z. Wang, A. C. Bovik, H. R. Sheikh, and E. P. Simoncelli. Image quality assessment: from error visibility to structural similarity. *IEEE Trans. Image Process.*, 13(4):600–612, 2004.
- Z. Wang, W. Yan, and T. Oates. Time series classification from scratch with deep neural networks: A strong baseline. In *Intl. Joint Conf. on Neural Networks*, pages 1578–1585, 2017.
- A. Warnecke, D. Arp, C. Wressnegger, and K. Rieck. Evaluating explanation methods for deep learning in security. In *IEEE European Symposium on Security and Privacy, EuroS&P*, pages 158–174, 2020.

- C.-K. Yeh, C.-Y. Hsieh, A. Suggala, D. I. Inouye, and P. K. Ravikumar. On the (in)fidelity and sensitivity of explanations. In *Advances in Neural Information Processing Systems*, volume 32, 2019.
- H. Zhang, Y. Yu, J. Jiao, E. P. Xing, L. E. Ghaoui, and M. I. Jordan. Theoretically principled trade-off between robustness and accuracy. In K. Chaudhuri and R. Salakhutdinov, editors, *Proceedings of the 36th International Conference on Machine Learning, ICML 2019, 9-15 June 2019, Long Beach, California, USA*, volume 97 of *Proceedings of Machine Learning Research*, pages 7472–7482. PMLR, 2019.
- Q. Zhang and S. Zhu. Visual interpretability for deep learning: a survey. *Frontiers Inf. Technol. Electron. Eng.*, 19(1):27–39, 2018.
- B. Zhou, A. Khosla, A. Lapedriza, A. Oliva, and A. Torralba. Learning deep features for discriminative localization. In *Proceedings of the IEEE Conference on Computer Vision and Pattern Recognition (CVPR)*, June 2016.